An international comparison of phase angle standards between the novel impedance bridges of CMI, INRIM and METAS

An international comparison of phase angle standards between the novel impedance bridges of CMI, INRIM and METAS

Massimo Ortolano[1,4], Luis Palafox[2], Jan Kučera[3], Luca Callegaro[4], Vincenzo D'Elia[4], Martina Marzano[1,4], Frédéric Overney[5] and Gülay Gülmez[6]

[1] Politecnico di Torino
Corso Duca degli Abruzzi 24, 10129 Torino, Italy
[2] PTB — Physikalisch-Technische Bundesanstalt
Bundesallee 100, D-38116 Braunschweig, Germany
[3]CMI — Czech Metrology Institute
Okruzni 31, 63800 Brno, Czech Republic
[4]INRIM — Istituto Nazionale di Ricerca Metrologica
Strada delle Cacce, 91, 10135 Torino, Italy
[5]METAS — Federal Institute of Metrology
Lindenweg 50, CH-3003 Berne-Wabern, Switzerland
[6]TÜBİTAK UME — Ulusal Metroloji Enstitüsü
Barış Mahallesi, TÜBİTAK Gebze Yerleşkesi, 41470 Gebze/Kocaeli, Turkey

E-mail: `massimo.ortolano@polito.it`

Abstract. We report here the results of a comparison of electrical impedance standards aimed at evaluating four novel digital impedance bridges developed by the national metrology institutes CMI, INRIM and METAS. This comparison, which is the first of its kind, involved phase angle impedance standards developed by TÜBİTAK UME with phase angles of $\pm30^\circ$ and $\pm60^\circ$, and magnitudes ranging from about $100\,\Omega$ to $1\,\mathrm{M}\Omega$. The comparison demonstrated agreement among the measurement results obtained with the different bridges, and allowed us to gather information on the stability of the phase standards and on the more critical aspects related to the characterization of the bridges.

PACS numbers: 06.20.fb, 06.30.Ka

Submitted to: *Metrologia*

1. Introduction

Electrical impedance is a quantity of interest for many applications, either as the main measurand or as the output quantity of a sensor [1]. In the former case, it is usually required to accurately measure the impedance magnitude (or magnitude and phase angle) of resistive, capacitive or inductive elements (or combinations thereof), where the elements can be in solid, liquid or gaseous form. In the latter, it is usually required to measure impedance changes, possibly with high resolution.

Traditionally, National Metrology Institutes maintain impedance units with scales composed of decadic values of resistance (R), capacitance (C), and inductance (L), having phase angles close to 0° or ±90°: that is, fixed points along the Cartesian axes of the complex impedance plane. Transformer-based bridges allow to perform unit linking and scaling with ultimate accuracy, but are complex and demanding instruments, requiring calibration at every operating frequency and a highly skilled operator performing long measurements. Transformer bridges are unsuitable to perform direct measurements of impedances of arbitrary magnitude and phase, which are instead measured with electronic LCR meters — calibrated against the maintained R, L and C scales, either directly or via secondary travelling standards, with a relevant increase in the measurement uncertainty.

In 2013, an international collaboration (see Acknowledgments) started to work on extending impedance measurements performed at predefined ratio values and selected frequencies to measurements of any ratio and phase values over any frequency in the audio range. Previous attempts to automate transformer bridges, and make them more flexible, resulted in a significant increase in uncertainty, due to the limitations introduced by controlling these devices remotely. The partners felt that modern digital signal generation techniques would allow significantly better performance than before, foreseeing to reach the level of uncertainty available from coaxial transformer-based impedance bridges.

The authors' aim is to expand the capabilities of the participating NMIs to measure intermediate values on the resistance, capacitance and inductance axes of the impedance complex plane and also to measure impedances with intermediate phase angles. Novel impedance bridges have been developed by CMI in Czech Republic, INRIM in Italy and METAS in Switzerland in order to reach these objectives. In order to test these novel measurement capabilities, TÜBİTAK UME developed impedance standards with magnitudes in the range between 100 Ω and 1 MΩ for phase angles of ±30° and ±60°.

The standards were measured at INRIM, METAS and CMI, in an informal indirect comparison of the impedance bridges at these intermediate phase angles. This is the first ever intercomparison of this type at the NMI level. In this paper, we describe the impedance bridges and the standards, and report and analyse the measurement results.

In the following, bridges are classified according to their type — fully digital (FD) or digitally assisted (DA) — and to the realized impedance definition — two terminal-pair (2TP) or four terminal-pair (4TP) [2].

2. CMI 4TP-FD, a four terminal-pair fully digital bridge

CMI 4TP-FD bridge performs ratio measurements of two four-terminal pair impedance standards. Details about the bridge together with a description of uncertainty sources are given in [3, 4]. The schematic of CMI 4TP-FD is depicted in figure 1. The two impedance standards whose impedance ratio is compared are denoted by Z_{A} and Z_{B}.

2.1. Bridge operation

The reference voltage ratio is formed by means of a two-channel generator with outputs G2A and G2B. The main balance of the bridge at point D1 is nulled by adjusting U_{GB} phase and amplitude (figure 1). The measured ratio of Z_{A} and Z_{B} can be derived from

$$\frac{Z_{\mathrm{B}}}{Z_{\mathrm{A}}} \approx \frac{U_{\mathrm{GB}}}{U_{\mathrm{GA}}}. \tag{1}$$

The ratio of measured impedances becomes equal to the ratio $U_{\mathrm{GB}}/U_{\mathrm{GA}}$ only when all conditions for the 4TP definition [2] are fulfilled. The zero current condition in the high potential arms of impedances Z_{A} and Z_{B} is achieved by adjusting the auxiliary current arms formed by G3A and G3B. The residual currents are detected by means of voltage measurements on the outputs of detection transformers TR1 and TR2 (points D3 and D4). The influence of the voltage drop across the current link between Z_{A} and Z_{B} is

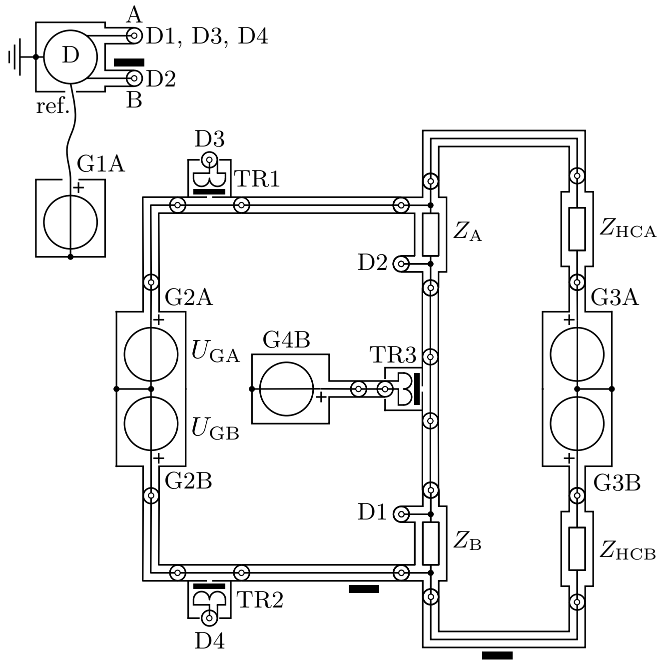

Figure 1. Coaxial schematic diagram of 4TP-FD bridge developed at CMI. Points denoted by Ei represent grounding points which are common to channels GiA and GiB of the ith generator. Black rings represent current equalizers.

minimized (i.e., the voltage difference between points D1 and D2 is maintained negligibly small) by means of the injection circuit TR3 which is energized from generator G4B. The current arms in the bridge drive the currents into the compared impedances Z_A and Z_B, nulling the loads of G2A and G2B in agreement with the 4TP definition of the impedances. This is crucial for the specification of their voltage ratio, especially when Z_A and Z_B have low nominal values. A lock-in amplifier with optional differential input mode serves as the null detector D and is synchronized with the generators by a reference signal from generator G1A.

The bridge balancing procedure consists of repeatedly setting generator outputs G2B, G3A, G3B and G4B in accordance to the residual voltages measured at points D1, D2−D1, D3 and D4. Measurement points Di are switched to the inputs of the lock-in amplifier during the balancing procedure with the help of a coaxial multiplexer.

2.2. Implementation

The accuracy of CMI 4TP-FD is specified mainly by the properties of the applied generators. CMI 4TP-FD is based on a set of two-channel modular sine wave generators (SWGs) developed at CMI [3], each with two highly accurate voltage sources GiA and GiB operating at RMS voltage levels up to 7 V. The SWG uses direct digital synthesis (DDS) to generate a sine wave signal. The DDS is implemented with a sine wave look-up table with high amplitude and angle resolutions together with 20 bit DACs to generate a pure sine wave signal with an optional 18 bit multiplying circuit to set the output amplitude. Additional fine tuning of the output amplitude is achieved by adjusting the reference voltage. This topology preserves a high spurious-free dynamic range even for small output amplitudes, which are necessary for measurements of small impedances. High voltage ratio stability of GiA and GiB is achieved by sharing the voltage reference between both voltage sources A and B in each generator module. Stable and adjustable phase shift of all generated signals necessary to energize and balance the bridge is achieved by synchronizing all SWGs from one external 10 MHz clock. The SWGs integrate several protections to prevent non-continuous changes in the sine wave signal across the connected devices. Communication and synchronization via optical fibres and optional operation from built-in battery packs minimize potential crosstalks between all SWGs. Because SWGs are battery operated, transformers without isolation between primary and secondary windings can be used within the bridge. The injection and detection transformers TR1,...,TR3 involved in the bridge are commercial, NL type, with ratios 100 : 1 or 1 : 100.

The null detector is a Signal Recovery SR 7280 lock-in amplifier. Measurement points Di are connected to the null detector via a CMI coaxial multiplexer with four independent, fully isolated channels [5]. This ensures negligible crosstalk between input and output of each opened switching channel (better than −185 dB for signals at 1 kHz, when both inner and outer conductors are opened). Each channel is controlled independently via an optical fibre.

The bridge balancing procedure is based on the secant method [6]. The first balancing iteration is evaluated from an initial bridge state and a programmatically unbalanced bridge state. The balancing procedure considers information from the null detector, bridge sensitivity, and voltage limits. To achieve balance for all conditions of the bridge, points Di are sequentially connected to the null detector by means of the coaxial multiplexer, the amount of unbalance is measured and the relevant injection voltage is evaluated by the control program. The bridge is usually balanced within three iterations of all injection and detector pairs within a few minutes.

The balancing procedure together with the control of the SWGs is implemented in a National Instruments (NI) LabView program. The overall uncertainty budget for the in-phase and quadrature parts of the measured ratio is evaluated by a Monte Carlo method in accordance with [7] and is also implemented in the LabView program.

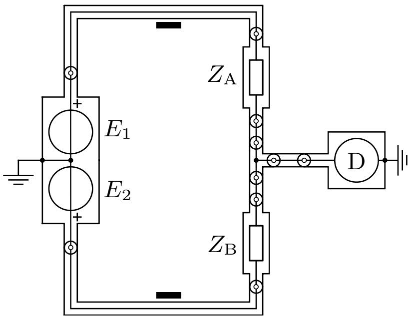

Figure 2. Coaxial schematic diagram of the INRIM 2TP-FD bridge (see section 3 for details). The black rectangles identify coaxial equalizers.

3. INRIM 2TP-FD, a two terminal-pair fully-digital bridge

INRIM 2TP-FD is a coaxial fully-digital voltage ratio bridge which performs ratios of two terminal-pair impedance standards. The bridge is described in full detail in [8], together with test measurements and an expression of the measurement uncertainty. Here we give a short summary of its operation and implementation.

3.1. Bridge operation

The schematic diagram of INRIM 2TP-FD, shown in figure 2, is well known in the literature (see [9, Ch. 5] and references therein; [10, 11]). A digital source with two channels, labelled 1 and 2, drives the impedances Z_{A} and Z_{B} to be compared, connected in series. The bridge balance is sensed by the detector D, and the balance is achieved by adjusting either E_1 or E_2 in magnitude and phase.

The bridge operates in *forward* mode when, as in figure 2, channel 1 is connected to Z_{A} and channel 2 to Z_{B}. We denote as $E_{1\mathrm{A}}$ and $E_{2\mathrm{B}}$ the equilibrium voltages for this mode of operation.

In the *reverse* mode of operation, the source channels are reversed: channel 2 is connected to Z_{A} and channel 1 to Z_{B}. We denote as $E_{2\mathrm{A}}$ and $E_{1\mathrm{B}}$ the equilibrium voltages for this mode of operation.

It can be shown [8] that the quantity

$$W^{(\mathrm{r})} = \left[\frac{E_{1\mathrm{A}}}{E_{2\mathrm{B}}}\,\frac{E_{2\mathrm{A}}}{E_{1\mathrm{B}}}\right]^{\frac{1}{2}}, \tag{2}$$

which is the geometric average of the forward and reverse bridge readings, is an estimate of the true impedance ratio $W = Z_{\mathrm{A}}/Z_{\mathrm{B}}$ that rejects the gain tracking error between the source channels, both in magnitude and in phase. $W^{(\mathrm{r})}$ is however sensitive to the errors caused by the channel non-linearities, and to the voltage partition effects caused by source loading. These effects are taken into account by calculated corrections and as contributions to the uncertainty budget [8]. Cable corrections [9, Sec. 2.4] are also applied.

3.2. Implementation

The measurements reported in this paper were performed with a 2-channel 16 bit specialized commercial digital source, the Aivon Oy DualDAC [12]. D is a Stanford Research mod. 830 lock-in amplifier.

The bridge operation is automated by control software. Amplitude and phase of each channel can be adjusted by recalculating and uploading new waveform samples. The readings are calculated from the Fourier expansions of the quantized waveforms. An automatic balancing routine [6, Sec. IV] is implemented: for a single mode, the balance time is usually less than 1 min.

4. INRIM 4TP-DA, a four terminal-pair digitally-assisted bridge

INRIM 4TP-DA is a three-arm current comparator digitally-assisted bridge that allows the comparison of *three* unlike impedance standards over the complex plane. The four terminal-pair definition of the three standards is approximated.

The bridge network and its implementation and operation are described in detail in [13] for a two terminal-pair version, and in [14, 15] for the present four terminal-pair version. The cited papers provide also examples of measurements and details about the uncertainty evaluation.

4.1. Bridge operation

The schematic diagram of INRIM 4TP-DA is given in figure 3. The bridge main elements are the voltage source E, providing the bridge excitation; the multi-tap current comparator CC; the three main arms $m = 1, \ldots, 3$, including a four terminal-pair admittance standard Y_m each; the injection arm 0, composed by the voltage source E_0 and the admittance Y_0; and the detector D, which senses the bridge main balance at the secondary winding of CC.

In addition, the auxiliary voltage sources E_{L} and E_{H}, and the auxiliary detectors $\mathrm{D_L}$ and $\mathrm{D_H}$, are employed to achieve a four terminal-pair definition of the compared admittances.

In the following, we consider Y_1 and Y_2 as calibrated standards and Y_3 as the measurand. Y_0 is also a known admittance standard.

CC is driven by the currents I_k, $k = 0, \ldots, 3$, crossing the injection arm 0 and the main arms $m = 1, \ldots, 3$. The main equilibrium is detected by D and is achieved by adjusting $I_0 = E_0 Y_0$. At equilibrium, the relationship $\sum_{k=0}^{3} n_k\, I_k = 0$ holds.

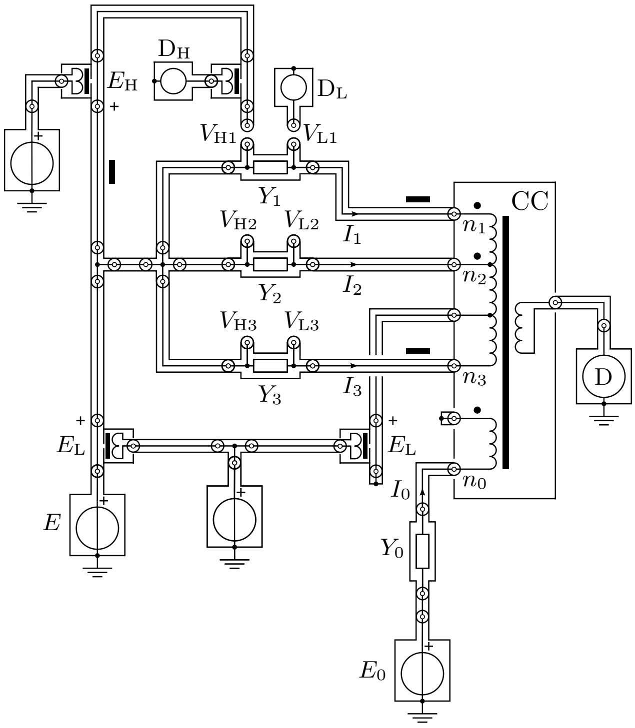

Figure 3. Schematic diagram of INRIM 4TP-DA(see section 4 for details).

The two tracking voltage sources E_L allow the adjustment of the low voltages $V_{\mathrm{L}m}$ of each Y_m without altering the bridge excitation, which is thus kept constant to E. Each $V_{\mathrm{L}m}$ can be measured by connecting $\mathrm{D_L}$ to the appropriate port.

The voltage source E_H and the synchronous detector $\mathrm{D_H}$ form a potentiometric arm measuring the voltage drop across the high side of the bridge, from the main excitation to each of the high-voltage ports $V_{\mathrm{H}m}$.

The bridge is configured by identifying the taps n_m that, for the particular admittances Y_m being compared, minimize the injection I_k with respect to the main current magnitudes $|I_m|$. The measurement procedure minimizes the average of $V_{\mathrm{L}m}$, thus achieving an approximate four terminal-pair definition of all three Y_m.

The measurement procedure consists of the following steps [15]:

1) Leaving unconnected the potentiometric arm composed by the source E_H and the detector $\mathrm{D_H}$, set $E_\mathrm{L} = 0$ and balance D by adjusting E_0.
2) For each Y_m connect the detector $\mathrm{D_L}$ to the low-voltage port $V_{\mathrm{L}m}$; adjust E_L to balance $\mathrm{D_L}$, $V_{\mathrm{L}m} = 0$; if the main balance D changes, readjust E_0 and E_L in turns until both D and $\mathrm{D_L}$ are balanced; and let then $E_{\mathrm{L}m}$ be the value of E_L for the admittance Y_m at the convergence of the two equilibria.
3) Set $E_\mathrm{L} = (\sum_{m=1}^{3} E_{\mathrm{L}m})/3$, to minimize the deviation of each low-voltage port from perfect four terminal-pair definition.
4) Recheck D and, whether necessary, readjust E_0.
5) For each Y_m, connect the potentiometric arm E_H-$\mathrm{D_H}$ to the high-voltage port $V_{\mathrm{H}m}$; balance $\mathrm{D_H}$ by adjusting E_H; and let $E_{\mathrm{H}m}$ be the value of E_H for the admittance Y_m when $\mathrm{D_H}$ is balanced.

From the above procedure, the following measurement equation can be derived [15], yielding Y_3 in terms of the standards Y_1, Y_2, and Y_0, the voltages E and E_0, and the voltage settings $E_{\mathrm{L}m}$ and $E_{\mathrm{H}m}$:

$$Y_3 = -\frac{n_1 Y_1 (E + E_\mathrm{L1} - E_\mathrm{H1}) + n_2 Y_2 (E + E_\mathrm{L2} - E_\mathrm{H2})}{n_3 (E + E_\mathrm{L3} - E_\mathrm{H3})} - \frac{n_0 Y_0 E_0}{n_3 (E + E_\mathrm{L3} - E_\mathrm{H3})}. \quad (3)$$

4.2. Implementation

The bridge employs a 7-channel 18 bit digital source specifically developed for this application at the University of Zielona Góra [16].

Voltages E_L and E_H are obtained from two channels through 200 : 1 feedthrough injection voltage transformers [9, Sec. 3.3.9]. The current comparator CC, which is described in detail in [17], is provided with a primary ratio winding having 21 taps corresponding to turn numbers $n = -100, -90, \ldots, +90, +100$, and an injection winding with $n_0 = 40$ turns. The 200-turn detection winding is doubly shielded (electrostatic and magnetic shields) from the other windings.

D is a single Stanford Research mod. 830 lock-in amplifier, manually switched across the positions D, $\mathrm{D_L}$ and $\mathrm{D_H}$. When in position $\mathrm{D_H}$, the detector is connected to the bridge through a 1 : 200 feedthrough transformer.

The main and auxiliary bridge balances are achieved with an automatic balancing algorithm [6]. The whole measurement procedure takes around 5–10 min.

5. METAS 4TP-FD, a four terminal-pair fully digital bridge

The schematic of METAS 4TP-FD, the fully digital bridge developed at METAS, is represented in figure 4. The two four terminal-pair impedance standards to be compared are Z_top and Z_bot.

5.1. Bridge operation

Balancing the bridge requires the use of three sources S_top, S_bot and S_K and three digitizers $V_\mathrm{bot}^\mathrm{LP}$, $V_\mathrm{top}^\mathrm{LP}$ and V_MUX. The amplitude of the source S_top is first adjusted to set the current flowing through the

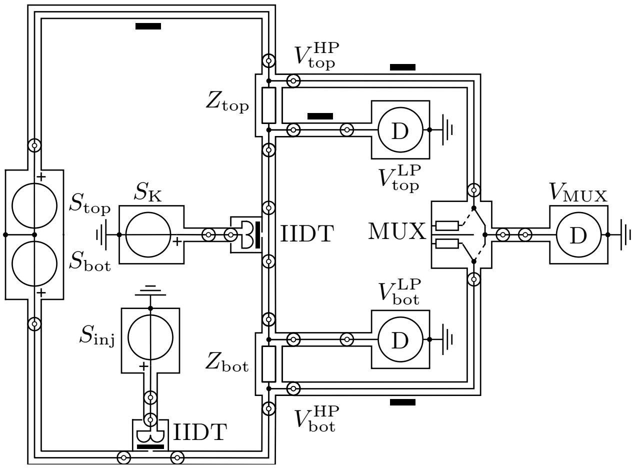

Figure 4. Schematic representation of the coaxial full digital bridge developed at METAS for the comparison of the four terminal-pair impedance standards $Z_{\rm top}$ and $Z_{\rm bot}$. The bridge contains four voltage sources ($S_{\rm top}$, $S_{\rm bot}$, $S_{\rm K}$ and $S_{\rm inj}$), three digitizers ($V_{\rm top}^{\rm LP}$, $V_{\rm bot}^{\rm LP}$ and $V_{\rm MUX}$), two isolated injection-detection transformers (IIDT) and one coaxial multiplexer (MUX). The use of four coaxial chokes ensures current equalization in each coaxial cable of the bridge.

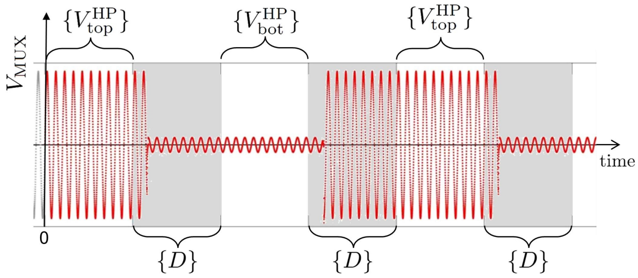

Figure 5. The output voltage of the MUX, sampled by the digitizer $V_{\rm MUX}$, is plotted as a function of time. The samples are grouped in sets of N values. When the MUX switches from one input channel to the other, the data set is discarded (gray zone data $\{D\}$). This process results in a sequence of data sets $\{V_{\rm top}^{\rm HP}\}$, $\{V_{\rm bot}^{\rm HP}\}$, $\{V_{\rm top}^{\rm HP}\}$, $\{V_{\rm bot}^{\rm HP}\}$, ... that can be used to calculate the ratio $V_{\rm bot}^{\rm HP}/V_{\rm top}^{\rm HP}$ as explained in the text.

impedance $Z_{\rm top}$ to the desired value. Then, the amplitude and phase of the sources $S_{\rm bot}$ and $S_{\rm K}$ are adjusted to bring the voltage measured by the two digitizers $V_{\rm top}^{\rm LP}$ and $V_{\rm bot}^{\rm LP}$ to zero. The balancing procedure is facilitated by considering the following auxiliary quantities: $V_{\rm MB} = \frac{1}{2}(V_{\rm top}^{\rm LP} + V_{\rm bot}^{\rm LP})$ and $V_{\rm K} = \frac{1}{2}(V_{\rm top}^{\rm LP} - V_{\rm bot}^{\rm LP})$. In fact, the so-called main balance $V_{\rm MB}$ is mainly dependent on $S_{\rm bot}$, whereas the so-called Kelvin balance $V_{\rm K}$ is mainly dependent on $S_{\rm K}$.

The supplementary source $S_{\rm inj}$ is optional and was implemented to increase the resolution of the main balance.

Once the bridge is balanced, i.e., once $V_{\rm MB} \approx 0$ and $V_{\rm K} \approx 0$, the four terminal-pair definition [2] of the impedance standards is realized and the impedances ratio is given by

$$\frac{Z_{\rm bot}}{Z_{\rm top}} = -\frac{V_{\rm bot}^{\rm HP}}{V_{\rm top}^{\rm HP}}. \tag{4}$$

Therefore, if the reference value of the impedance $Z_{\rm top}$ is known, the modulus and phase of an unknown impedance $Z_{\rm bot}$ can be obtained by the precise measurement of the voltage ratio $V_{\rm bot}^{\rm HP}/V_{\rm top}^{\rm HP}$.

The measurement of the voltage ratio is performed by sampling the voltages $V_{\rm bot}^{\rm HP}$ and $V_{\rm top}^{\rm HP}$ using the single digitizer $V_{\rm MUX}$ and the multiplexer MUX. This technique [18] implies that the two voltages are not measured simultaneously but successively. The main advantage of successive sampling is that the gain error of the digitizer cancels out in the ratio calculation as long as it is stable during the time needed to measure the two voltages. This time is typically around 300 ms in our setup.

The voltage applied to the digitizer $V_{\rm MUX}$ and the data processing leading to the determination of the voltage ratio are represented in figure 5 and are fully described in [19]. The output voltage of the MUX is continuously sampled and the values are grouped by data sets of N values with no lost values between two successive data sets. During the sampling of the two channels, three data sets containing N values each are sampled: the first one during the measurement of $V_{\rm top}^{\rm HP}$, the second one during the switching between the two voltages (this one is of course discarded) and the third one during the measurement of $V_{\rm bot}^{\rm HP}$. At the end, a sequence of useful data sets, $\{V_{\rm top}^{\rm HP}\}$, $\{V_{\rm bot}^{\rm HP}\}$, $\{V_{\rm top}^{\rm HP}\}$, $\{V_{\rm bot}^{\rm HP}\}$, ... therefore remains.

Each data set contains $P = Nf/f_{\rm s}$ periods of the measured signal. For a given signal at a frequency f, N and $f_{\rm s}$ are chosen to achieve a coherent sampling, i.e., P is an integer greater than 2. A discrete Fourier transform (DFT) is then applied to each useful data set. The P's component of the DFT gives information on the amplitude and phase of the fundamental component of the measured signal. Combining two successive DFTs leads to the determination of the voltage ratio and therefore, the unknown impedance, $Z_{\rm bot}$, is finally given by

$$Z_{\rm bot} = -Z_{\rm top}\frac{{\rm DFT}_N\{V_{\rm bot}^{\rm HP}\}}{{\rm DFT}_N\{V_{\rm top}^{\rm HP}\}}. \tag{5}$$

5.2. Implementation

The stability of the two sources $S_{\rm top}$ and $S_{\rm bot}$ determines the accurate realization of the main balance $V_{\rm MB} \approx 0$. Therefore, the 24 bit DACs used in previous implementations [20, 21] were replaced by a high stability 16 bit commercial source [12]. The requirements on the sources $S_{\rm inj}$ and $S_{\rm K}$ are less critical and the DAC outputs of a NI PXI-4461 board were used.

The digitizers $V_{\mathrm{top}}^{\mathrm{LP}}$, $V_{\mathrm{bot}}^{\mathrm{LP}}$ and V_{MUX} are each an input channel (24 bit ADC) of two NI PXI-4461 boards. One NI PXI-4461 board has 2 output channels and 2 input channels. Therefore, the bridge of figure 4 requires two NI PXI-4461 boards in total.

The two IIDTs are bespoke transformers with 100 turns at the primary winding and 1 turn at the secondary winding. A double electrostatic shield was placed between the primary and secondary windings to avoid any leakage current between the bridge circuit and the DAC sources.

Coaxial chokes [22] were also implemented, one in each mesh of the bridge, to ensure current equalization and the immunity of the bridge to external interferences [23].

The bespoke multiplexer, MUX, has two coaxial input channels and one coaxial output channel. To avoid current redistribution between the two phases of the measurement [20], the unused input channel is connected to a shorting impedance (see figure 4) whose value is adjusted to be the same as the input impedance of the digitizer measuring V_{MUX}. The switching signals controlling the state of the MUX are supplied by an NI PXI-2567 board.

The whole system is fully computer controlled and a LabView program manages the balancing procedure [24, 6] as well as the measurement of the voltage ratio. The time required to carry out the calibration of one standard at a given frequency is typically less than 6 min.

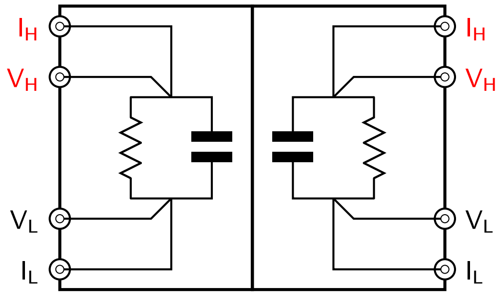

(a)

(b)

Figure 6. Schematic (a) of the negative phase standards and photograph (b) of the 0097 standard. The box in figure (b) contains two phase standards: in this paper, the standard on the left is identified with the suffix “A”; the one the right, with the suffix “B”. The sockets labelled *Temp. Control* and *Temp. Indicator* are connected to two thermistors sensing the box temperature, one for the external temperature controller and one for the operator.

6. TÜBİTAK UME standards

The standards employed during the comparison have been specifically designed to have, at the measurement frequency of 1 kHz, nominal phase angles of ±30° and ±60°, impedance magnitudes from 100 Ω to 1 MΩ, and a 4TP connection configuration.

The negative (*RC*) phase standards 0097, 0098, 0099 are assembled in boxes according to the schematic of figure 6(a). Each box contains two independent standards, with phase angles of −30° or −60°, identified in this paper with the suffixes “A” and “B”. The standards employ wirewound resistors (Vishay S106 series) and C0G capacitors (AVX SkyCap SR Series, Kemet Goldmax 300 series and Multicomp MCRR series) mounted on a printed circuit board. Figure 6(b) shows a picture of the standard 0097.

The positive (*RL*) phase standards 0103 and 0104 are assembled in boxes according to the schematic of figure 7(a), which allows to obtain two different phase angles (+30° and +60°) with a single inductor. Each box includes one commercial air-core toroidal inductance standard (IET Labs mod. 1482-P, 1 H, and 1482-H, 10 mH) and two metal-foil resistors (Vishay Z201 series). Each standard is identified in this paper with the suffix “A” or “B”.

The nominal values of the components employed in the standards are given in table 1.

All standard boxes are temperature controlled with an active heating controller. Each box contains two NTC thermistor API mod. GB1074U-3-0: one (*Temp. Control* in figures 6(b) and 7(b)) is used exclusively by the temperature controller, connected externally, whereas the other (*Temp. Indicator* in figures 6(b) and 7(b)) is available to the operator for temperature monitoring. The connectors to the thermistors are visible in figures 6(b) and 6(b). The heating power is delivered by flexible heaters Omega mods. KHLV-202/2-P and SRFG-406/2-P. The analog proportional-integrative controller, described in [25], is housed in an independent box. The temperature

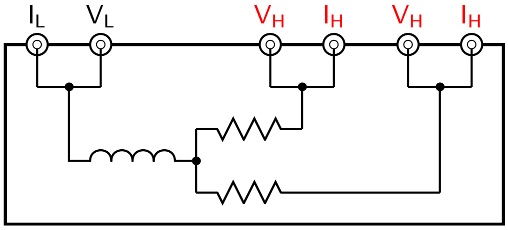

(a)

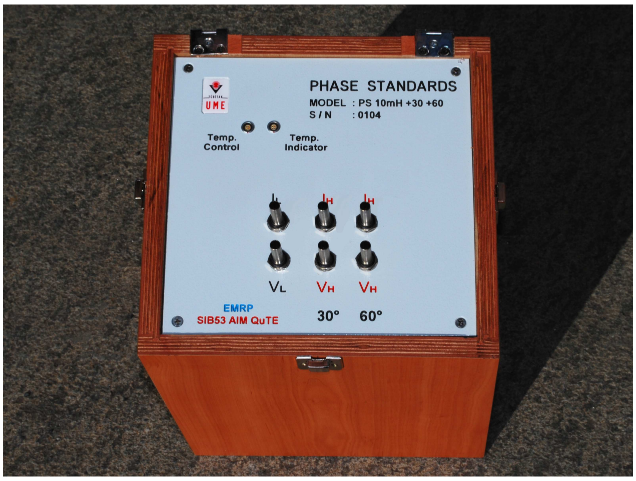

(b)

Figure 7. Schematic (a) of the positive phase standards and photograph (b) of the 0104 standard. As for the negative standards, the box in figure (b) contains two phase standards, which are identified in this work with the suffixes "A" (left) and "B" (right). The sockets labelled *Temp. Control* and *Temp. Indicator* are connected to two thermistors sensing the box temperature, one for the external temperature controller and one for the operator.

stability, monitored over a time of 10 days, was better than $\pm 10\,\mathrm{mK/day}$. The temperature stability is further discussed in Appendix B.

7. Results

7.1. Outline of the comparison

The standards described in section 6 were measured by the participating NMIs, although not all the NMIs were able to measure all the standards due to time constraints, as reported in table 1. INRIM measured the standards at the beginning and at the end of the comparison.

In this section we shall present and discuss the results in graphic form. A spreadsheet, listing raw and corrected data, is available from a dedicated page [26] on the project website.

The standards were measured at the nominal frequency $f_0 = 1\,\mathrm{kHz}$. The impedance values $Z(f)$ reported by each institute were adjusted to the frequency f_0 to compensate for variations of the working frequency f across the measurements. The adjustment was performed as described in Appendix A. The operating temperature of the standards was recorded for almost all measurements‡. The temperature stability of the standards and their temperature coefficients are evaluated in Appendix B; overall, temperature effects are negligibly small.

The bridges used in the comparison implemented different impedance definitions (two terminal-pair, with or without cable corrections, and four terminal-pair). Results are compared among measurements performed with the same impedance definition.

Figure 8 reports the results for the standards 0097A/B; figure 9, those for the standards 0098A/B; figure 10, those for the standards 0099A/B; figure 11, those for the standards 0103A/B; and figure 12, those for the standards 0104A/B. Uncertainty bars have been drawn according to a coverage factor $k = 2$.

Some results which are of particular interest are those obtained with the bridges INRIM 2TP-FD and METAS 4TP-FD on the standards 0097A/B, 0098A/B and 0103A/B during an INRIM-METAS bilateral comparison carried out at METAS in January, 2016. In this case, the measurements were performed over a short time period and the same impedance definition (two terminal-pair) and reference standards were employed for both the INRIM and METAS bridges. The results of this bilateral comparison are marked with a black triangle in figures 8, 9 and 11.

7.2. Behaviour of the standards

The duration of the comparison was of almost 3 years. No previous information was available on the long-term and travelling stability of these devices. We performed a simple analysis of the possible drifts by considering the initial and the final measurements obtained with INRIM 2TP-FD (INRIM 4TP-DA for standards 0104A and 0104B). Table 2 reports the estimated drift coefficients for the magnitude and the phase of the measured standards.

Standards 0097A/B, 0098A/B, 0099B, 0103A/B appear to have drifted significantly — in magnitude or phase — during the comparison period. Standards 0099A and 0104A/B do not show appreciable drift.

7.3. Uncertainty and discussion

The amount of reported measurements and the number of different measurement systems do not allow to discuss the associated uncertainty budgets. Details about the uncertainty sources considered for each bridge are discussed in [3, 4, 8, 13, 24]. Common uncertainty sources include contributions due to:

‡ The operating temperature was not recorded for the standards 0104A/B.

Table 1. Composition of the standards and nominal phase angles at 1 kHz. The symbols + and || denote, respectively, series and parallel connection. In the last three columns, the bullets indicate which standards were measured by each institute.

Standard model no.	Impedance composition	Nominal phase	CMI 4TP-FD	INRIM 2TP-FD	INRIM 4TP-DA	METAS 4TP-FD
0097A	9.189 kΩ || 10 nF	−30°	•	•	•	•
0097B	91.89 kΩ || 1 nF	−30°	•	•	•	•
0098A	102.7 kΩ || 2.7 nF	−60°		•	•	•
0098B	10.21 kΩ || 27.5 nF	−60°		•	•	•
0099A	999.7 kΩ || 92.4 pF	−30°		•	•	•
0099B	999.6 kΩ || 275 pF	−60°		•	•	•
0103A	3.64 kΩ + 1 H	+60°		•	•	•
0103B	10.87 kΩ + 1 H	+30°		•	•	•
0104A	108.7 Ω + 10 mH	+30°			•	•
0104B	36.7 Ω + 10 mH	+60°			•	•

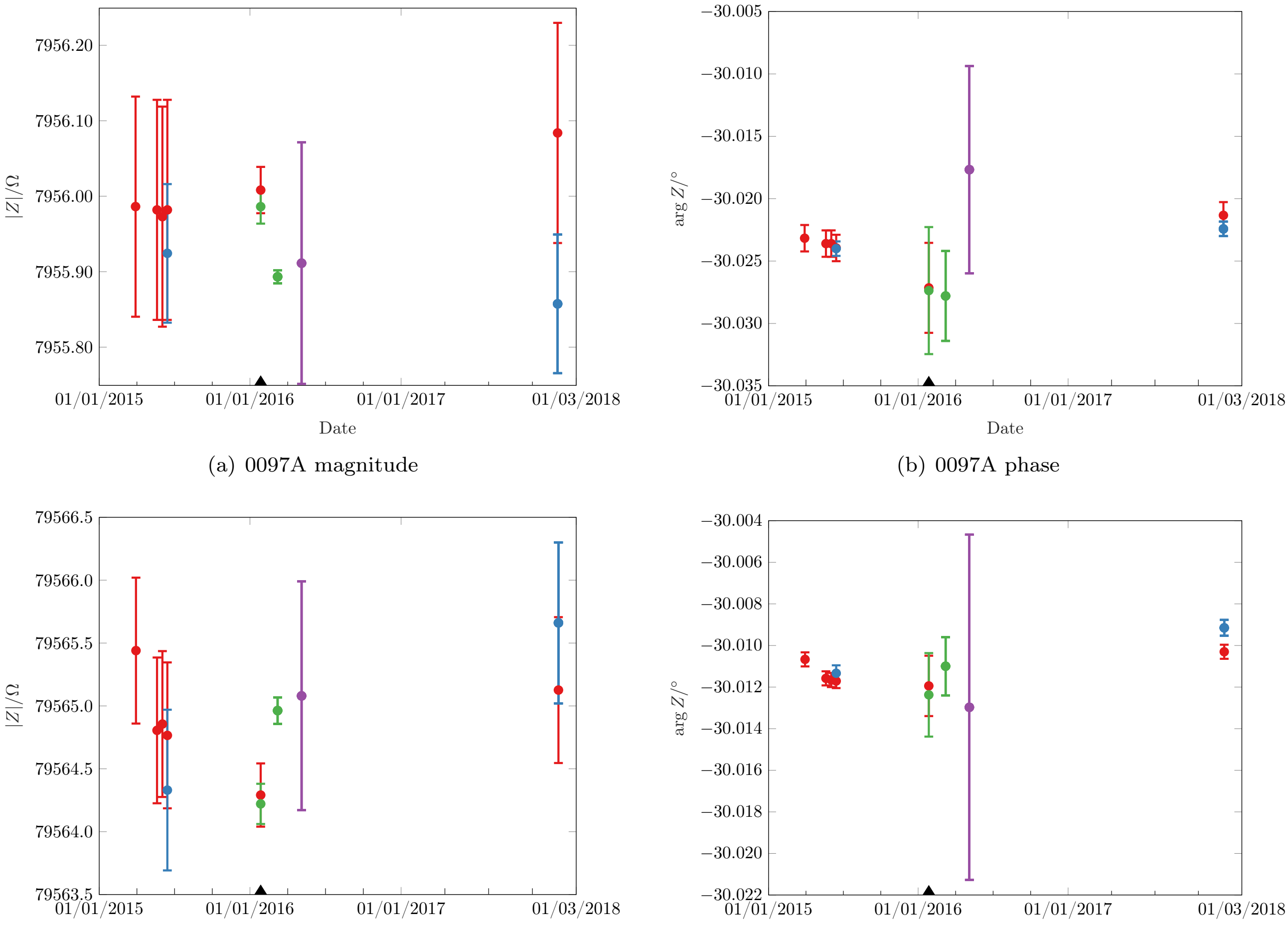

(a) 0097A magnitude

(b) 0097A phase

(c) 0097B magnitude

(d) 0097B phase

Figure 8. Results for the *RC* standards 0097A and 0097B: —— INRIM 2TP-FD; —— INRIM 4TP-DA; —— METAS 4TP-FD; —— CMI 4TP-FD. Uncertainty bars correspond to a coverage factor $k = 2$. The black triangle marks the results obtained during the INRIM-METAS bilateral comparison on January 27, 2016.

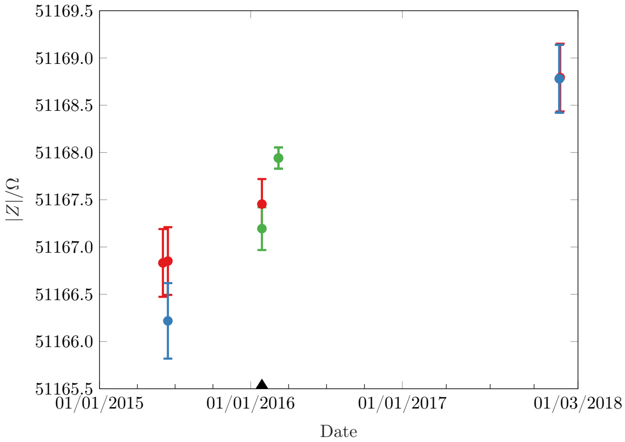

(a) 0098A magnitude

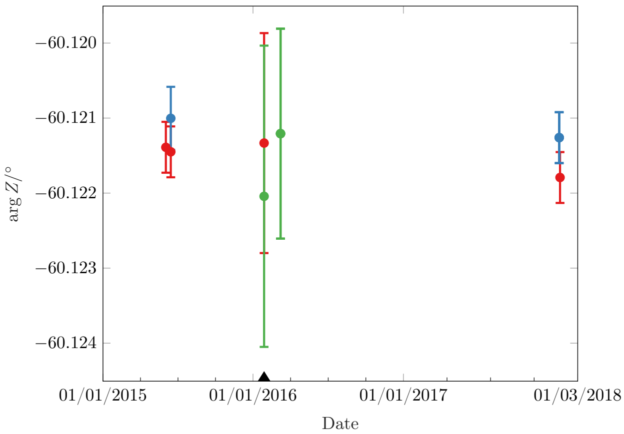

(b) 0098A phase

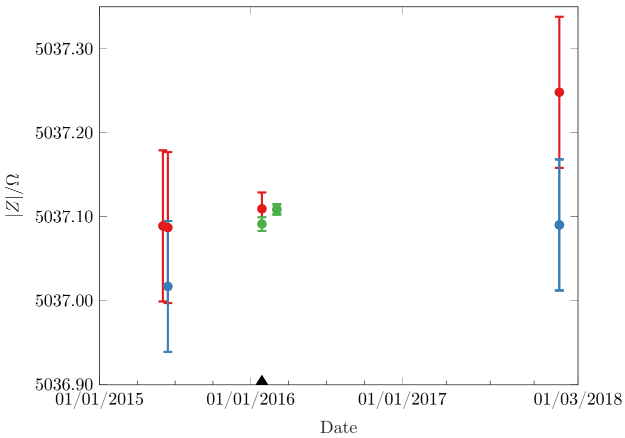

(c) 0098B magnitude

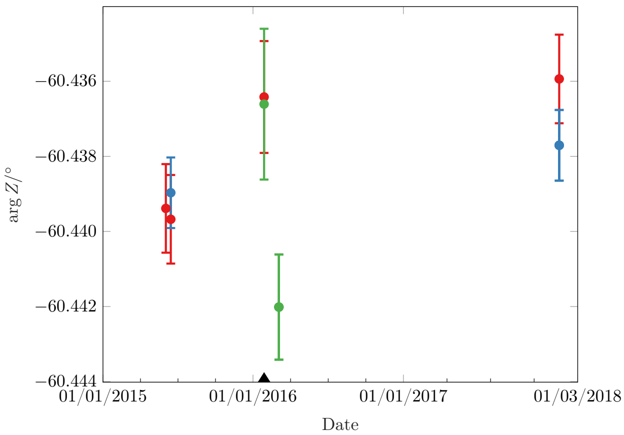

(d) 0098B phase

Figure 9. Results for the *RC* standards 0098A and 0098B: INRIM 2TP-FD; INRIM 4TP-DA; METAS 4TP-FD. Uncertainty bars correspond to a coverage factor $k = 2$. The black triangle marks the results obtained during the INRIM-METAS bilateral comparison on January 28, 2016.

Table 2. Estimated drift coefficients of magnitude and phase of the measured standards. The uncertainty is specified with a coverage factor $k = 2$.

Standard model no.	$\lvert Z\rvert^{-1}\,\mathrm{d}\lvert Z\rvert/\,\mathrm{d}t$ (10^{-6}/year)	$\mathrm{d}\arg Z/\,\mathrm{d}t$ (µrad/year)
0097A	5 ± 10	18 ± 10
0097B	2 ± 4	10 ± 3
0098A	15 ± 4	-2 ± 3
0098B	12 ± 10	25 ± 11
0099A	0 ± 4	-3 ± 3
0099B	11 ± 4	6 ± 3
0103A	-47 ± 11	-37 ± 15
0103B	-12 ± 11	-31 ± 13
0104A	4 ± 136	6 ± 79
0104B	41 ± 154	15 ± 26

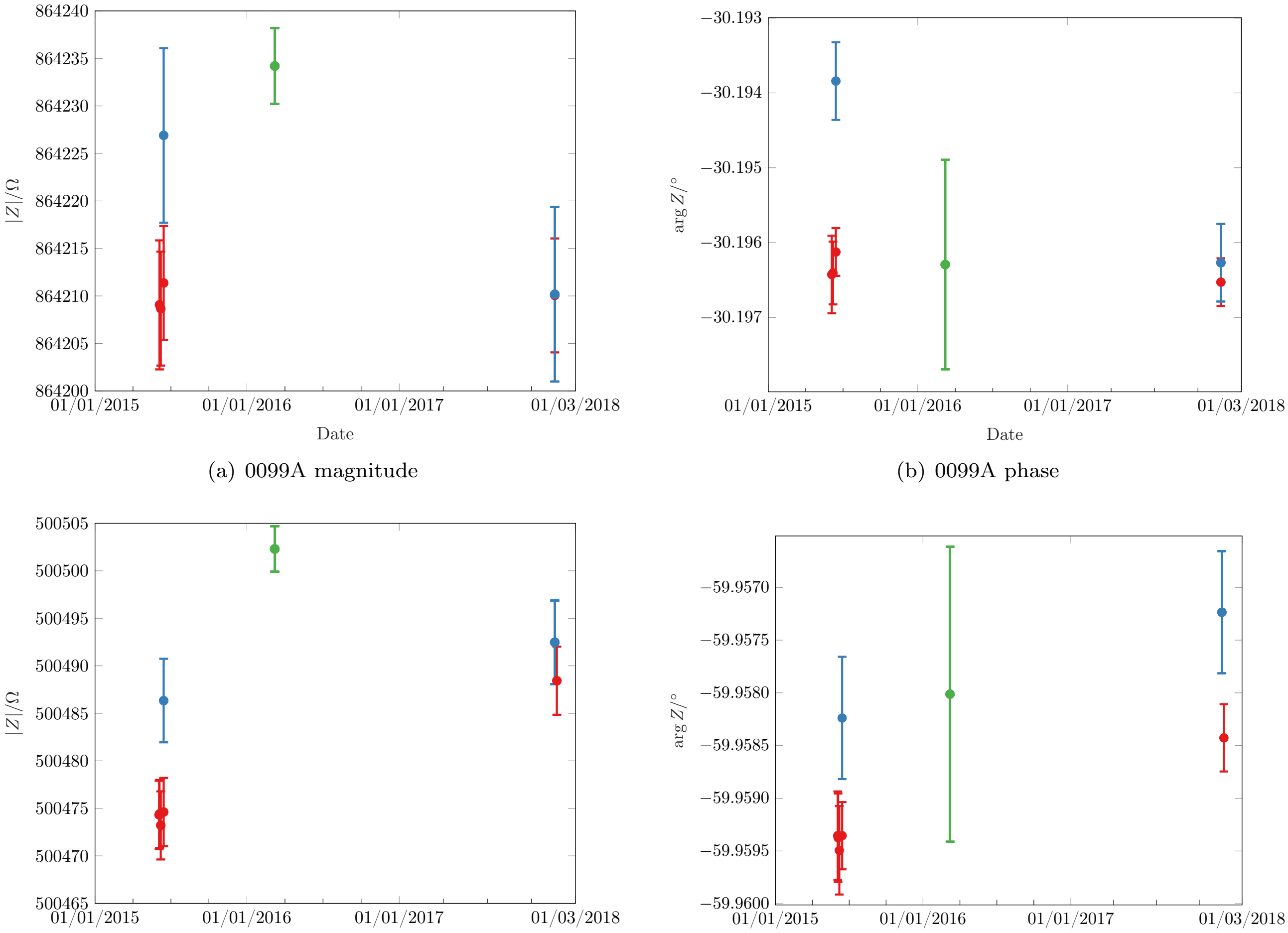

(a) 0099A magnitude

(b) 0099A phase

(c) 0099B magnitude

(d) 0099B phase

Figure 10. Results for the *RC* standards 0099A and 0099B: — INRIM 2TP-FD; — INRIM 4TP-DA; — METAS 4TP-FD. Uncertainty bars correspond to a coverage factor $k = 2$.

Standards The complex reference values of the standards employed in each measurement enter the measurement model, and both the uncertainty of the primary parameter (e.g., the capacitance for a capacitor) and of the secondary parameter (e.g., dissipation factor) are of relevance.

Impedance definition Each bridge realizes to a certain degree the 2TP or 4TP impedance definition of the standards involved. In particular, INRIM 4TP-DA explicitly relies on an approximated impedance definition. Uncertainty in the cable corrections of 2TP measurements has to be also taken into account.

Converter errors Fully-digital bridges and, to a lesser extent, digitally-assisted bridges rely on the accuracy of the digital representations of the physical sinusoidal voltage waveforms. Quantization error of the converters; magnitude and phase errors of the gain, nonlinearity, and crosstalk of the converters and of the related analog electronics are of concern. Measurement procedures (e.g., channel swapping) have been developed to mitigate the effects of some of these errors.

Transformer ratio errors Digitally-assisted bridges rely on current or voltage transformers for operation: the calibration uncertainty of the complex ratio enters the measurement model.

Correction terms Bridge measurement models can include correction terms that are evaluated for the specific measurement point.

Noise The measurement repeatability of each bridge is expressed as a Type A uncertainty contribution for each measurement outcome.

These sources contribute to the overall uncertainty through complex sensitivity coefficients whose magnitude and phase are highly dependent on the bridge type and working point. In most cases, the main contribution to the reported uncertainty is that of the indi-

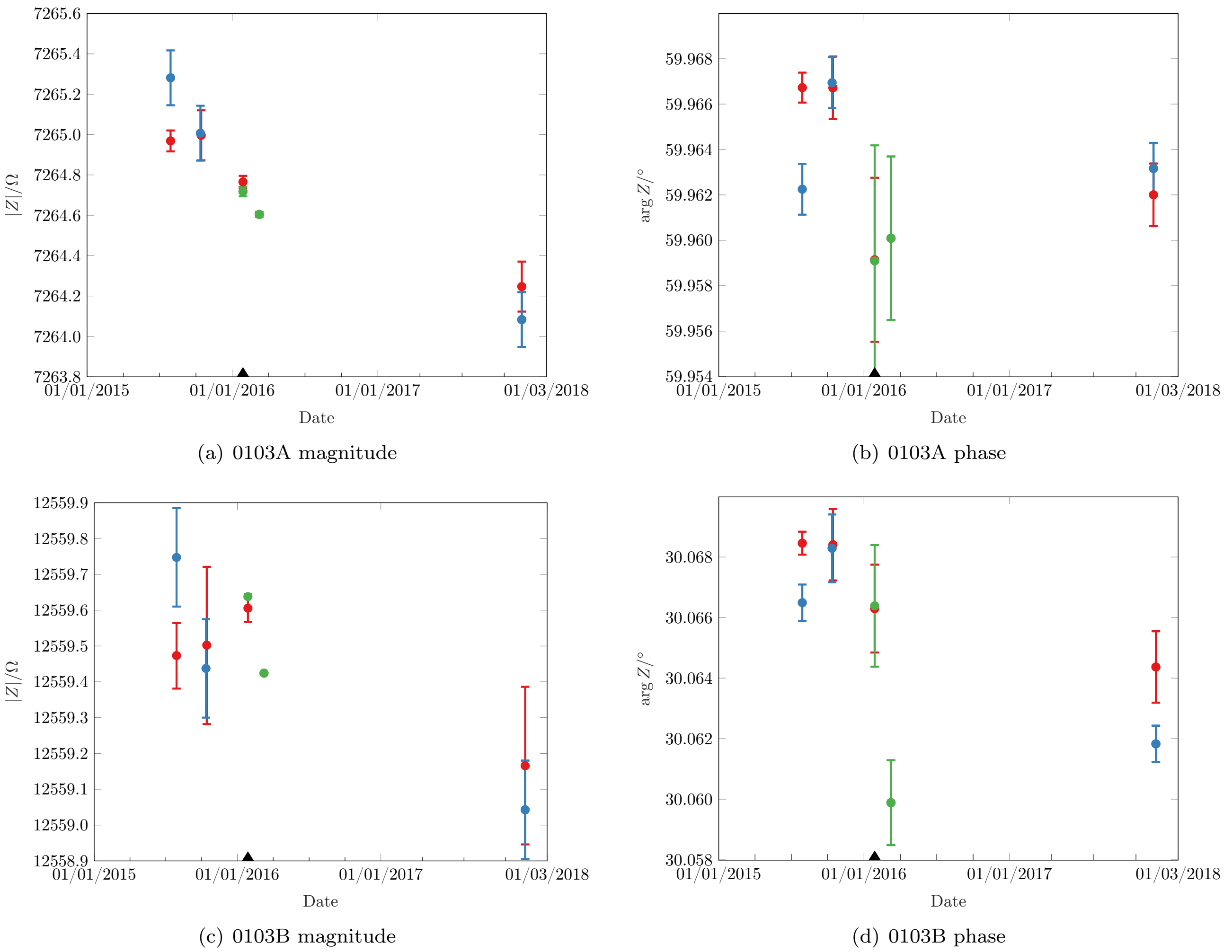

Figure 11. Results for the *RL* standards 0103A and 0103B: — INRIM 2TP-FD; — INRIM 4TP-DA; — METAS 4TP-FD. Uncertainty bars correspond to a coverage factor $k = 2$. The black triangle marks the results obtained during the INRIM-METAS bilateral comparison on January 28, 2016.

vidual calibrated standards used as reference (usually, resistors and capacitors). In particular, the phase angle uncertainty is dominated by the uncertainty of the secondary parameters of the reference standards. All this generates the variability of the uncertainty bars in figures 8–12.

The uncertainties reported are mostly in the 10^{-6}–10^{-5} range for the magnitude and at a level of few tens of microradians for the phase angle.

For the INRIM-METAS bilateral comparison (measurements marked with a black triangle in the figures), the differences between the results are within 7×10^{-6} for the magnitude and 14 µrad for the phase, and are compatible with the reported uncertainties. In this particular case, both the INRIM and the METAS bridges were operated with the same reference standards. These measurements, however, will not be compared to the other measurements of the full comparison because they were taken with the bridges configured for a different impedance definition, that is, two terminal-pair with cables and no cable correction.

The results of the full comparison show a reasonable compatibility; when occurring, the discrepancies are limited within 2–3 times the combined uncertainty. These discrepancies might be related to the instability of the phase standards, and to an underestimation of certain uncertainty contributions to individual measurements. For what concerns the intrinsic uncertainty of the bridges, we point out a non exhaustive characterization of converters gain and nonlinearity. Furthermore, the good outcome of the bilateral comparison suggests that there can be discrepancies in the maintained impedance scales of the NMIs involved for what concerns the secondary parameters, not verified in recent international intercomparisons.

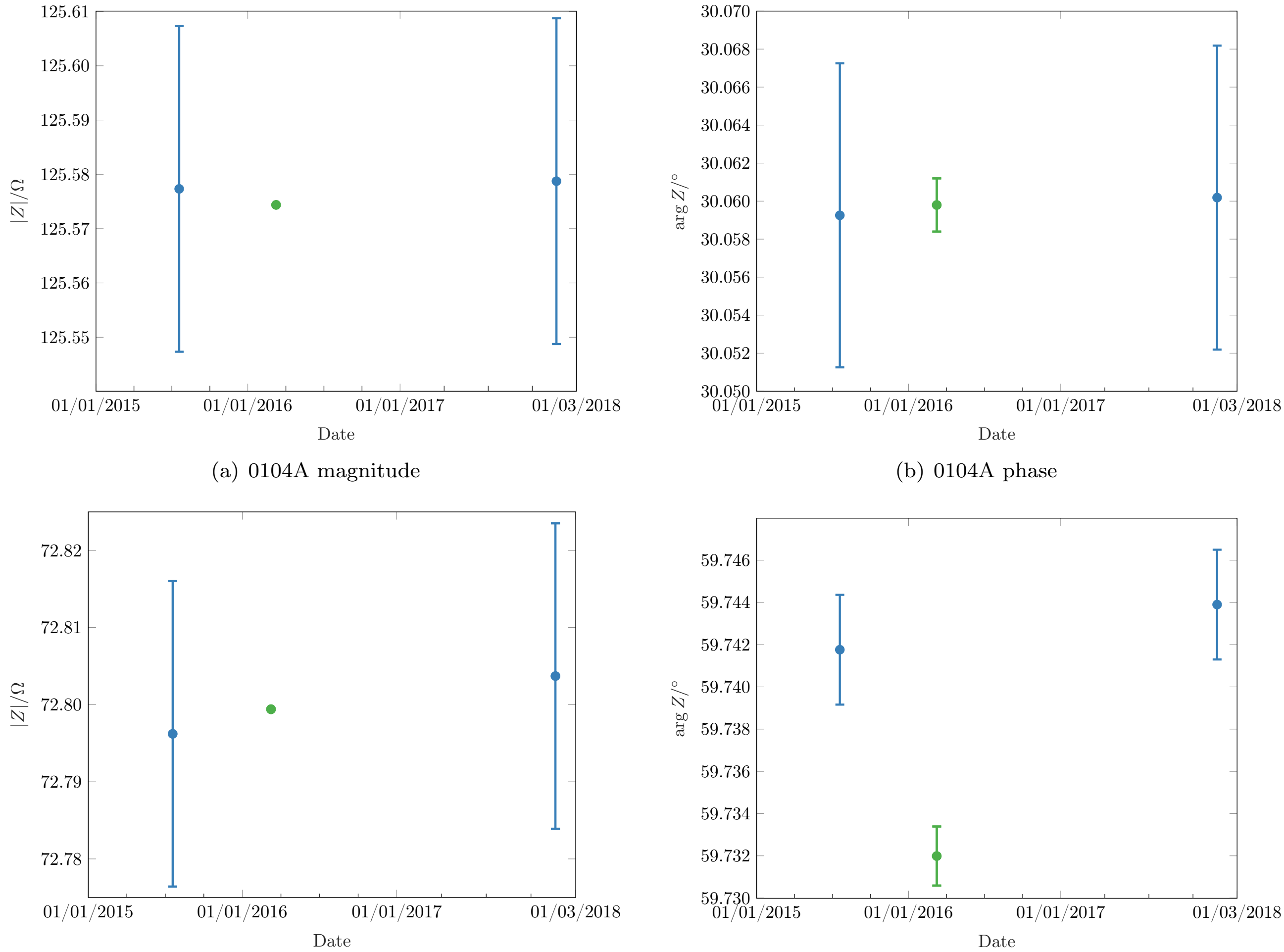

(a) 0104A magnitude (b) 0104A phase

(c) 0104B magnitude (d) 0104B phase

Figure 12. Results for the *RL* standards 0104A and 0104B: INRIM 4TP-DA; METAS 4TP-FD. Uncertainty bars correspond to a coverage factor $k = 2$.

8. Conclusions

This paper reviewed the impedance bridges developed by CMI, INRIM and METAS during the EMRP Project SIB53 AIM QuTE and presented the results of a comparison among them. For the first time, four different implementations of digital coaxial impedance bridges based on different measurement techniques and different equipment were compared. The comparison was realized by means of travelling phase angle impedance standards, specifically developed for this task by TÜBİTAK UME. These results show that digital impedance bridges are mature for primary metrology, yielding accurate measurements over the whole complex plane with simpler and faster operating procedures with respect to transformer-based bridges.

Acknowledgements

This work was carried out within the EMRP Project SIB53 AIM QuTE, “Automated impedance metrology extending the quantum toolbox for electricity”. The EMRP is jointly funded by the EMRP participating countries within EURAMET and the European Union. The project, running from 2013 to 2016, brought together National Metrology Institutes (NMIs) from Spain, Czech Republic, Italy, France, Switzerland, Poland, Finland, Germany, Sweden, Denmark and Turkey and a German calibration laboratory. A full description of the project is presented in [27] and on the project website [28].

The authors are indebted with Marian Kampik, Silesian University of Technology, Poland, and Dan Bee Kim, Korea Research Institute of Standards and Science, Korea, for their contribution in the implementation of INRIM 2TP-FD; Ryszard Rybski and Janusz

Kaczmarek, University of Zielona Góra, Poland, for the development of the source employed in INRIM 4TP-DA; Faranak Pourdanesh, INRIM and Politecnico di Torino, Italy, contributed to the implementation of both INRIM 2TP-FD and INRIM 4TP-DA; Jakub Kovac, CMI, for the development of the sources employed by CMI.

Appendix A. Frequency adjustment

The frequency adjustment has been performed by modelling the impedances as parallel RC or series RL circuits with constant component values, according to their composition. This model is acceptable when the deviation of f with respect to f_0 is relatively small.

The standards 0097A/B, 0098A/B and 0099A/B have been modelled as parallel RC circuits; the adjustment equation is

$$Z(f_0) = \frac{1}{\operatorname{Re}\left[\frac{1}{Z(f)}\right] + \mathrm{j}\operatorname{Im}\left[\frac{1}{Z(f)}\right]\frac{f_0}{f}}. \tag{A.1}$$

The standards 0103A/B and 0104A/B have been modelled as series RL circuits; the adjustment equation is

$$Z(f_0) = \operatorname{Re}[Z(f)] + \mathrm{j}\operatorname{Im}[Z(f)]\frac{f_0}{f}. \tag{A.2}$$

To evaluate the significance of the adjustments and their contribution to the measurement uncertainty, we can approximate the magnitude $|Z(f_0)|$ and the phase angle $\varphi(f_0) = \arg Z(f_0)$ with a first-order Taylor series expansion in the relative frequency deviation $\Delta f/f_0 = (f - f_0)/f_0$.

For the magnitude, equations (A.1) and (A.2) yield

$$|Z(f_0)| \approx |Z(f)|\left[1 \pm \frac{\Delta f}{f_0}\sin^2\varphi(f)\right], \tag{A.3}$$

with the plus sign for the RC model and the minus sign for the RL one. For the phase angle, both equations yield

$$\varphi(f_0) \approx \varphi(f) - \frac{1}{2}\frac{\Delta f}{f_0}\sin 2\varphi(f). \tag{A.4}$$

For the standards 0097A/B, 0098A/B and 0099A/B, the magnitude adjustment is at most of few parts in 10^6; the phase angle adjustment is at most of 2 µrad. The contributions of these adjustments to the uncertainties of magnitude and phase angle are completely negligible.

In the case of the standards 0103A/B and 0104A/B, INRIM performed some of the measurements at a frequency of about 1003 Hz to limit the effect of a power line interference. For these measurements, the corrections are of the order of 10^{-3} relatively to the magnitude and 1 mrad for the phase angle. The contributions of these adjustments to the uncertainties of magnitude and phase angle are negligible at the uncertainty level declared by INRIM for these standards.

Appendix B. Temperature stability

Knowledge of the temperature coefficients of the standards allows to estimate the maximum impedance variations across the measurements caused by temperature instability. The temperature coefficients are here estimated from the specifications of the elements composing the standards. Experimental data are also reported for the RC standards.

For the RC standards 0097A/B, 0098A/B and 0099A/B, the temperature coefficients $\alpha(|Z|)$ and $\alpha(\varphi)$ of, respectively, magnitude and phase can be written as

$$\alpha(|Z|) \approx \frac{1}{\Delta T}\frac{\Delta|Z|}{|Z|} \approx \alpha(R)\cos^2\varphi - \alpha(C)\sin^2\varphi \tag{B.1}$$

and

$$\alpha(\varphi) \approx \frac{\Delta\varphi}{\Delta T} \approx \frac{1}{2}[\alpha(R) + \alpha(C)]\sin(2\varphi), \tag{B.2}$$

where $\alpha(R)$ is the temperature coefficient of the resistance, $\alpha(C)$ is the temperature coefficient of the capacitance and ΔT is the temperature variation.

For the RL standards 0103A/B and 0104A/B, the temperature coefficients of magnitude and phase can be written as

$$\alpha(|Z|) \approx \alpha(R)\cos^2\varphi + \alpha(L)\sin^2\varphi \tag{B.3}$$

and

$$\alpha(\varphi) \approx \frac{1}{2}[-\alpha(R) + \alpha(L)]\sin(2\varphi), \tag{B.4}$$

where $\alpha(L)$ is the temperature coefficient of the inductance.

For the capacitors, $|\alpha(C)| < 3 \times 10^{-5}$/K; for the inductors, $\alpha(L) \approx 3 \times 10^{-5}$/K; and for the resistors, $\alpha(R)$ is of the order of 10^{-6}/K, which is relatively negligible.

Table B1 reports the estimated limits (worst case) and the measured temperature coefficients of magnitude and phase for the RC standards.

Table B2 reports, for each standard where temperature data were available, the maximum temperature variation observed between different measurements, the estimated maximum relative magnitude variation and the estimated maximum phase angle variation.

References

[1] L. Callegaro, "Traceable measurements of electrical impedance," *IEEE Instrum. Meas. Mag.*, vol. 18, pp. 42–46, 2015.

Table B1. Estimated limits and measured temperature coefficients of magnitude and phase for the *RC* standards.

	$\alpha(\lvert Z\rvert)/(10^{-6}/\mathrm{K})$		$\alpha(\varphi)/(^\circ/\mathrm{K})$	
Standard	Limits	Measured	Limits	Measured
0097A	± 9	-3.4	± 0.80	≈ 0
0097B	± 9	-8.6	± 0.80	-8.0×10^{-4}
0098A	± 23	6.1	± 0.80	7.1×10^{-4}
0098B	± 23	-2.1	± 0.80	-8.0×10^{-4}
0099A	± 9	-9.7	± 0.80	-5.0×10^{-4}
0099B	± 23	-24.4	± 0.80	-8.0×10^{-4}

Table B2. Maximum estimated impedance variations due to temperature variations across the measurements. For each standard, the second column reports the maximum temperature variation observed between different measurements; the third column, the estimated maximum relative magnitude variation; and the fourth column, the estimated maximum phase angle variation.

Standard	$\lvert\Delta T\rvert/\mathrm{mK}$	$\lvert\Delta\lvert Z\rvert\rvert/\lvert Z\rvert \times 10^6$	$\lvert\Delta\varphi\rvert/^\circ$
0097A	60	0.5	4.6×10^{-5}
0097B	60	0.5	4.6×10^{-5}
0098A	80	1.8	5.7×10^{-5}
0098B	80	1.8	5.7×10^{-5}
0099A	40	0.3	2.9×10^{-5}
0099B	40	0.9	2.9×10^{-5}
0103A	40	0.9	2.9×10^{-5}
0103B	40	0.3	2.9×10^{-5}

[2] R. D. Cutkosky, "Four-terminal-pair networks as precision admittance and impedance standards," *IEEE Transactions on Communication and Electronics*, vol. 83, no. 70, pp. 19–22, 1964.

[3] J. Kučera and J. Kováč, "A reconfigurable four terminal-pair digitally assisted and fully digital impedance ratio bridge," in *Proceedings of the 2017 IEEE International Instrumentation and Measurement Technology Conference (I^{2}MTC 2017)*, 2017, pp. 674–679.

[4] ——, "A reconfigurable four terminal-pair digitally assisted and fully digital impedance ratio bridge," *IEEE Trans. Instrum. Meas.*, vol. 67, 2018, in press.

[5] J. Kováč and J. Kučera, "A modular coaxial multiplexer with high isolation between channels," in *Proceedings of the 21st IMEKO World Congress*, Prague, Czech Republic, Aug, 30 – Sep, 4 2015, pp. 596–600.

[6] L. Callegaro, "On strategies for automatic bridge balancing," *IEEE Trans. Instrum. Meas.*, vol. 54, pp. 529–532, 2005.

[7] "JCGM 102:2011, Evaluation of measurement data — Supplement 2 to the "Guide to the expression of uncertainty in measurement" — Extension to any number of output quantities," 2011. [Online]. Available: http://www.bipm.org

[8] L. Callegaro, V. D'Elia, M. Kampik, D. Kim, M. Ortolano, and F. Pourdanesh, "Experiences with a two-terminal-pair digital impedance bridge," *IEEE Trans. Instrum. Meas.*, vol. 64, pp. 1460–1465, 2015.

[9] L. Callegaro, *Electrical impedance: principles, measurement, and applications*, ser. in Sensors. Boca Raton, FL, USA: CRC press: Taylor & Francis, 2013, iSBN: 978-1-43-984910-1.

[10] D. B. Kim, K.-T. Kim, M.-S. Kim, K. M. Yu, W.-S. Kim, and Y. G. Kim, "All-around dual source impedance bridge," in *2012 Conference on Precision Electromagnetic Measurements (CPEM 2012)*, Washington DC, USA, Jul, 1–6 2012, pp. 592–593.

[11] J. Lan, Z. Zhang, Z. Li, Q. He, J. Zhao, and Z. Lu, "A digital compensation bridge for *R-C* comparisons," *Metrologia*, vol. 49, no. 3, p. 266, 2012.

[12] J. Nissilä, K. Ojasalo, M. Kampik, J. Kaasalainen, V. Maisi, M. Casserly, F. Overney, A. Christensen, L. Callegaro, V. D'Elia, N. T. M. Tran, F. Pourdanesh, M. Ortolano, D. B. Kim, J. Penttilä, and L. Roschier, "A precise two-channel digitally synthesized AC voltage source for impedance metrology," in *2014 Conference on Precision Electromagnetic Measurements (CPEM 2014)*, Aug, 24–29 2014, pp. 768–769.

[13] L. Callegaro, V. D'Elia, M. Ortolano, and F. Pourdanesh, "A three-arm current comparator bridge for impedance comparisons over the complex plane," *IEEE Trans. Instrum. Meas.*, vol. 64, pp. 1466–1471, 2015.

[14] M. Ortolano, V. D'Elia, and L. Callegaro, "A three-arm four terminal-pair digitally-assisted current comparator bridge for the comparison of arbitrary complex impedances," in *2016 Conference on Precision Electromagnetic Measurements (CPEM 2016)*, Ottawa, Canada, Jul, 10–15 2016, pp. 1–2.

[15] ——, "A three-arm four terminal-pair digitally-assisted current comparator bridge for the comparison of arbitrary complex impedances," *IEEE Trans. Instrum. Meas.*, vol. 66, pp. 1496–1502, 2017.

[16] J. Kaczmarek, R. Rybski, and M. Kozioł, "The polyphase ac voltage source for digital impedance bridges," in *Final dissemination workshop of EMRP projects AIM QuTE, GraphOhm and Q-WAVE*, Prague, 18–19 May 2016. [Online]. Available: https://www.ptb.de/emrp/sib53-finalworkshop.html

[17] B. Trinchera, V. D'Elia, and L. Callegaro, "A digitally assisted current comparator bridge for impedance scaling at audio frequencies," *IEEE Trans. Instrum. Meas.*, vol. 62, pp. 1771–1775, 2013.

[18] G. Ramm, H. Moser, and A. Braun, "A new scheme for generating and measuring active, reactive, and apparent power at power frequencies with uncertainties of 2.5x10-6," *IEEE Trans. Instrum. Meas.*, vol. 48, no. 2, pp. 422–426, 1999.

[19] F. Overney and B. Jeanneret, "Calibration of an LCR-Meter

at Arbitrary Phase Angles using a Fully Automated Impedance Simulator," *IEEE Trans. Instrum. Meas.*, vol. 66, pp. 1516–1523, 2017.

[20] ——, "Realization of an inductance scale traceable to the quantum Hall effect using an automated synchronous sampling system," *Metrologia*, vol. 47, no. 6, pp. 690–698, dec 2010.

[21] ——, "*RLC* Bridge Based on an Automated Synchronous Sampling System," *IEEE Trans. Instrum. Meas.*, vol. 60, no. 7, pp. 2393–2398, jul 2011.

[22] D. N. Homan, "Applications of coaxial chokes to A-C bridge circuits," *Journal of Research of the National Bureau of Standards, Section C: Engineering and Instrumentation*, vol. 72C, no. 2, p. 161, apr 1968.

[23] S. A. Awan, B. Kibble, and J. Schurr, *Coaxial Electrical Circuits for Interference-Free Measurements*, ser. IET electrical measurement series. Institution of Engineering and Technology, jan 2011.

[24] F. Overney, F. Lüönd, and B. Jeanneret, "Broadband fully automated digitally assisted coaxial bridge for high accuracy impedance ratio measurements," *Metrologia*, vol. 53, no. 3, pp. 918–926, jun 2016.

[25] Y. Gülmez, C. Gülmez, E. Turhan, and T. Özkan, "Temperature control system for inductance standard," in *2000 Conference on Precision Electromagnetic Measurements (CPEM 2000)*, Sydney, Australia, May 2000, pp. 143–144.

[26] "EMRP SIB53 AIM QuTE dataset," Online. [Online]. Available: https://www.ptb.de/emrp/fileadmin/documents/aimqute/AIMQuTE_CMI_INRIM_METAS_comparison_results.xls

[27] L. Palafox, F. Raso, J. Kučera, F. Overney, L. Callegaro, P. Gournay, A. Ziołek, J. Nissilä, G. Eklund, T. Lippert, Y. Gülmez, P. Fleischmann, M. Kampik, and R. Rybski, "AIM QuTE: Automated impedance metrology extending the quantum toolbox for electricity," in *International Congress of Metrology*, 2013, p. 11001.

[28] "EMRP SIB53 AIM QuTE home page," Online. [Online]. Available: http://www.ptb.de/emrp/aimqute.html